

# The Development and Testing of a Recuperator for a Solar Hybrid Micro Gas Turbine System

M.F. Afeltra  
S.J. van der Spuy, J.E. Hoffmann  
Department of Mechanical and Mechatronic Engineering,  
Stellenbosch University  
Centre for Renewable and Sustainable Energy Studies

## Abstract

The thermal efficiency of an MGT (micro gas turbine) system at Stellenbosch University was intended to be improved with the incorporation of a locally developed recuperator. A clamped plate, counter-flow design was chosen due to its simplicity. An effectiveness of 0.92 was desired and formed the design constraint on which to optimise the recuperator geometry. From this geometry a detailed design was performed. The recuperator was assembled, attached to the system and tested. To compare and validate the experimental results of the standard and recuperated MGT system, a Flownex model was developed. This large effectiveness value was not achievable, both practically and financially. An effectiveness of 0.6 was designed for instead. During experimentation, the MGT system could not self-sustain due to the additional pressure drops incurred by the recuperator, which were attributed to flow-maldistribution within the headers. A decoupled mode of testing was performed to evaluate effectiveness and cold-flow pressure drop of the recuperator. Close correlation of the experimental results was achieved analytically and with Flownex. Partial recuperation, with a bypass on the hot and cold-side, was modelled in Flownex and revealed that the system could self-sustain in this manner. An improved recuperator design is therefore proposed.

*Keywords:* Plate Heat Exchanger, Recuperator, Solarised, Flownex, Turbocharger

## 1. Introduction

MGTs (micro gas turbines) can be used to power off-grid regions and replace diesel generators, reducing emissions and running costs. Coupled with South Africa's excellent solar resource, SHMGTs (solar hybrid micro gas turbines) provide a better means of dispatching electricity more efficiently, with a lower carbon footprint. Recuperation of an MGT system can further reduce the fuel consumption, reducing fuel costs and emissions (Saravanamuttoo, et al., 2017). Furthermore, recuperation brings the compressed air temperature closer to the receiver inlet design temperature. The solar receiver would need less DNI (direct normal irradiation) input from the sun and can be made less complex, reducing cost (le Roux, et al., 2011). Recuperation offers the possibility to reduce cost, emissions and complexity in other system components while providing a more efficient cycle (Shah & Sekulić, 2003; Saravanamuttoo, et al., 2017; McDonald, 2000).

An MGT was developed at Stellenbosch University by Ssebabi (2020) using off-the-shelf turbocharger technology. A simple schematic of the system, adapted from Saravanamuttoo, et al., (2017), is illustrated in Figure 1. The turbochargers are designated according to the BorgWarner model names: "K31" and "K44". The MGT system is arranged in a twin-shaft setup where the K31 turbocharger acts as the gas generator and the K44 turbocharger consists of the power turbine and load for the system. The system currently has a relatively low experimental thermal efficiency of 3 to 4%. This efficiency can be improved with the incorporation of a recuperator. The clamped plate-style, counterflow recuperator concept developed by Dellar (2019) was chosen to be adapted for use in the current system, due to its simplicity and cost-effectiveness. The design criteria of McDonald (2000), where the effectiveness of the recuperator must be above 90% and the overall incurred pressure drop must be less than 5% of the compressor delivery pressure, were set as design constraints.



Ssebabi (2020) of 0.92, was used as a design constraint. Given an effectiveness value, the NTU for a counterflow heat exchanger can be calculated with (Çengel & Ghajar, 2015):

$$NTU = \frac{1}{1-c} \ln \left( \frac{\epsilon-1}{\epsilon c-1} \right); \quad c < 1 \quad (1)$$

where  $\epsilon$  is the effectiveness and  $c$  is the heat capacity ratio. The total heat transfer surface area can be written as the product of the NTU, minimum heat capacity ratio and the overall heat transfer coefficient, demonstrated in Equation (2). Fouling was accounted for on the air-side ( $R_{f,a}$ ) and exhaust-side ( $R_{f,g}$ ) heat transfer surfaces. These fouling factors were chosen to be 0.0004 and 0.018 m<sup>2</sup>K/W for the air-side and exhaust-side, respectively (Çengel & Ghajar, 2015). A wide channel width accompanied by a narrow channel height, to maintain compactness, is desirable. For a fully developed laminar flow (to be verified) with a constant wall flux and a channel aspect ratio of  $a/b \gg 8$ , the Nusselt number (Nu) is 8.24 (Çengel & Ghajar, 2015).

$$A_s = (NTU)C_{min} \left( \frac{2ab}{Nu(a+b)} \left( \frac{1}{k_a} + \frac{1}{k_g} \right) + R_{f,a} + R_{f,g} + \frac{t}{k_w} \right) \quad (2)$$

The variables  $k_a$ ,  $k_g$  and  $k_w$  are the thermal conductivities of the air, exhaust gas and plate. Conveniently, the surface area can be written as

$$A_s = (2N)aL \quad (3)$$

where  $N$  is the number of channel pairs. This is a useful relation because combinations of the parameters on the right-hand-side of the equation can be varied accordingly to arrive at a desired  $A_s$ . Alternatively, with a known  $A_s$  and one known parameter on the right-hand-side, the two remaining parameters can be varied. Noting that these parameters dictate the height, width and length of the recuperator, a combination can be chosen to remain within the space requirements of the MGT system.

The pressure drop relation for plate heat exchangers developed by Kays & London (2018), was adapted to include the friction factor for laminar flow with  $a/b \gg 8$  and with the channel length rewritten in terms of surface area, channel width and number of channel pairs. The final relation, for one fluid side of the recuperator, is presented in the equation below. The first term is the header pressure drop, estimated as 1.5 times the inlet velocity head, the second term is the core pressure drop and the last term accounts for the sudden momentum change due to expansion and contraction into and from the core of the recuperator.

$$\Delta P = \frac{12\dot{m}^2}{\pi^2 D_p^4 \rho_i} + \frac{6\mu_m A_s \dot{m} (a+b)^2}{N^2 \rho_m a^4 b^3} + \left( \frac{1}{\rho_o} - \frac{1}{\rho_i} \right) \frac{\dot{m}^2}{(Nab)^2} \quad (4)$$

In this relation  $\dot{m}$  is mass flow rate,  $\rho_i$ ,  $\rho_m$  and  $\rho_o$  are the inlet, mean and outlet densities, respectively. The diameter of the header is represented by  $D_p$  and the dynamic viscosity, by  $\mu_m$ . The stress and deflection of the recuperator plates cannot be ignored, especially when plates with a large width are needed for a favourable effectiveness. The maximum stress and deflection of the plates are given by the following formulae, respectively (Young & Budynas, 2002). The material choice for the recuperator was stainless-steel 316.

$$\sigma_{max} = \frac{0.5qa^2}{t^2} \quad (5)$$

$$\delta_{max} = \frac{0.0284qa^4}{Et^3} \quad (6)$$

In these equations,  $q$  is the pressure differential that acts over the plate and  $E$  is the Young's modulus of the material. The properties of stainless steel were evaluated at the exhaust temperature, determined through the process spoken about next.

A realistic operating point of the system was needed on which to base the heat transfer and pressure drop calculations. The operating point needed to be representative of the additional pressure drop incurred by the recuperator, the K31 compressor exit air temperature and pressure and K44 turbine exhaust temperature. For stainless-steel recuperators, the maximum exhaust gas inlet temperature should not be much above 627 °C (Saravanamuttoo, et al., 2017). Preliminary testing of the MGT system was conducted to obtain this operating point, where a valve upstream of the combustion chamber was slightly closed to simulate a flow restriction upstream of the compressor. The results of this test are presented in the table below.

**Table 1. Results from Standard MGT Testing**

rp	Exhaust Temperature [°C]	Compressor Outlet Temperature [°C]	$\dot{m}_a$ [kg/s]	$\dot{m}_F$ [kg/s]	$N_{K31}$ [RPM]
1.75	627	99	0.188	0.004	61,915

Large channel aspect ratios are desirable for heat transfer performance, however wider channels of lower plate thickness values have unacceptable deflections when narrow channel heights are desired. Hypothetical-equally separated spacers were included, as recommended by Dellar (2019), to overcome the deflection caused by the pressure difference between the cold and hot-sides, by dividing the channel width into smaller segments. This allowed a large channel width to be selected however, the number of spacers needed to be chosen carefully alongside the thickness of the plates. For a certain channel width, a lower plate thickness would require more spacers to limit deflection. This would entail the manufacture and assembly of more parts, which is undesirable as stipulated by McDonald (2000). Additionally, the cost of the plates increases with the thickness. Therefore, a balance between plate thickness and the number of spacers was required. It was found that a channel width of 0.2 m, accompanied by three spacers would be feasible for the recuperator.

The ideal gas properties of air were used on both fluid sides of the recuperator. At this stage, the reduced fuel mass flow rate due to recuperation was not known and air properties were assumed on the hot-side of the recuperator. With the desired effectiveness and operating state of the recuperator known, the remaining geometrical parameters could be varied to arrive at the corresponding heat transfer surface area. Figure 3(a) illustrates that the plate thickness affected the required heat transfer area minimally, while an increase of 0.5 mm in channel height is followed by an increase in 10 m<sup>2</sup> in surface area. Therefore, a gasket thickness in the lower range was desirable for maintain compactness and limiting cost.

The maximum allowable overall pressure drop of the system was determined using the stipulations of McDonald (2000), where 5% of the compressor's outlet pressure, at the selected operating point, equates to 8.9 kPa. With a fixed channel width, the three geometrical parameters that affected pressure drop were channel height, length and number of channel pairs. As previously mentioned, the number of channel pairs was related to channel length through the surface area, therefore; the core pressure drop and size of the recuperator could be evaluated simultaneously. This relation is presented in Figure 3(b). The discharged air from the compressor has to travel upwards to the combustion chamber, therefore; a logical decision was to stand the recuperator vertically. This set the compactness limit because it was desired to have a recuperator length that fit vertically in-between the K31 compressor outlet and the combustion chamber inlet. With a channel height of 0.9 mm, a balance between pressure drop, channel length and number of channel

pairs was found. At 125 channel pairs, the overall core pressure drop was 4.56 kPa, which corresponded to a channel length of 0.49 m. The dotted lines in Figure 3(b) illustrate how to read off a pressure drop and channel length for a certain number of channel pairs and channel height. It was confirmed that the flow remained laminar on both sides of the recuperator for the geometry selection process.

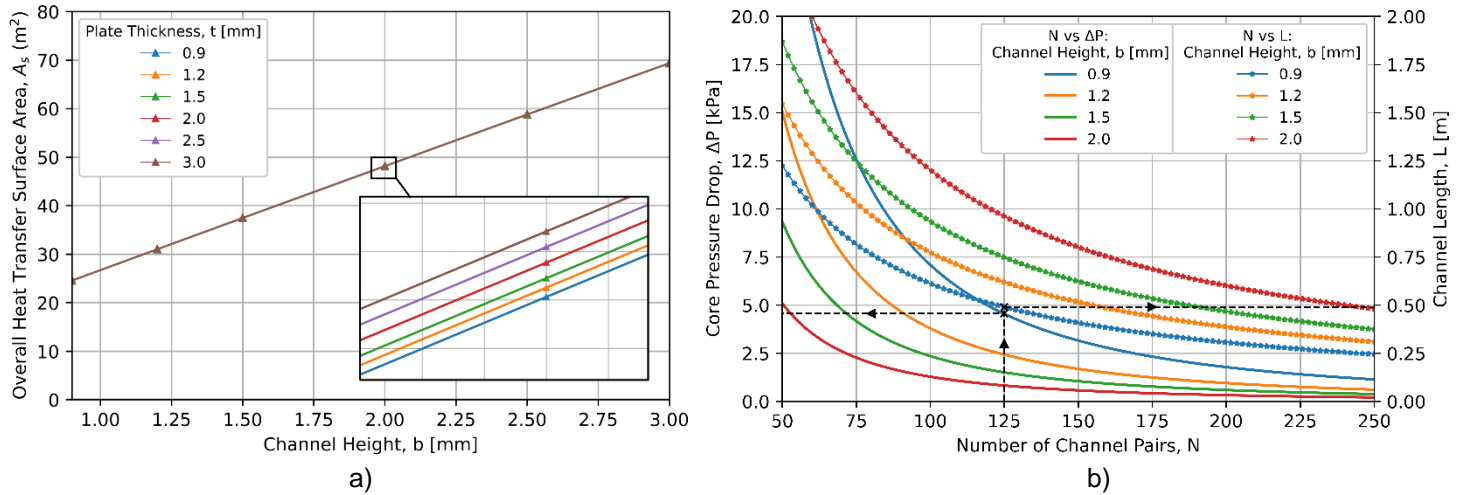


**Figure 3. a) Channel Height vs Overall Heat Transfer Surface Area, b) Number of Channel Pairs vs Core Pressure Drop and Channel Length**

A retrospective investigation of the heat loss analysis using the adapted equations from Nellis & Pfotenhauer (2005) with an ambient temperature of 30 °C, revealed a negligibly small effectiveness difference between the adiabatic and the HL (heat loss) model. This can be attributed to the vast heat transfer surface area within the recuperator, due to a large channel width, compared to the side areas of the recuperator that are losing heat to the environment.

The diameter of the inlet headers was selected in such a way as to minimise pressure drop and to not have an excessively large and impractical piping network. It was found that an inlet header diameter of 135.8 mm provided a sufficiently low overall pressure drop for both the cold and hot inlet header of 0.4 kPa. Additionally, this choice was aided by the K44 turbine's outlet diameter of 135 mm, which meant a continuous diameter pipe could be fitted in between the K44 exhaust and the hot-inlet to the recuperator.

### 3. Design and Implementation

The design of the gasket is presented in Figure 4(a). The flow passage was designed with large radius curves at the inlet to and exit from the core. This design decision was made in an attempt to guide the flow smoothly as it travels from/to a header, minimising flow separation off the wall of the gasket. A gasket width of 20 mm was chosen to be the minimum width separating the two flows from each other and the environment. This relatively large gasket width creates a larger length through which the gases must travel to escape, thus lowering the probability of a leak.

The spacers only needed to be implemented on half the number of the plates (Figure 4(b)) because the hot-side contains the lower pressure. The centre spacer was designed to be shorter because the channel width narrows as a header is approached, consequently, the plate deflection in this region is decreased. The shape of the spacers was designed to follow the flow direction and guide the flow along the length of the plate. Figure 4(c) provides an illustration of the flow paths on the hot and cold-sides of the recuperator. A U-flow header configuration was chosen. This arrangement minimises flow reversal and produces a more

uniform flow distribution over the heat exchanger core (Shah & Sekulić, 2003). The top and bottom flow channels were both chosen to contain air to minimise losses to the environment.

The outlet or combining header diameter was designed to be larger than the inlet or dividing header diameter. This design choice further attempts to minimise flow maldistribution within the core (Shah & Sekulić, 2003).

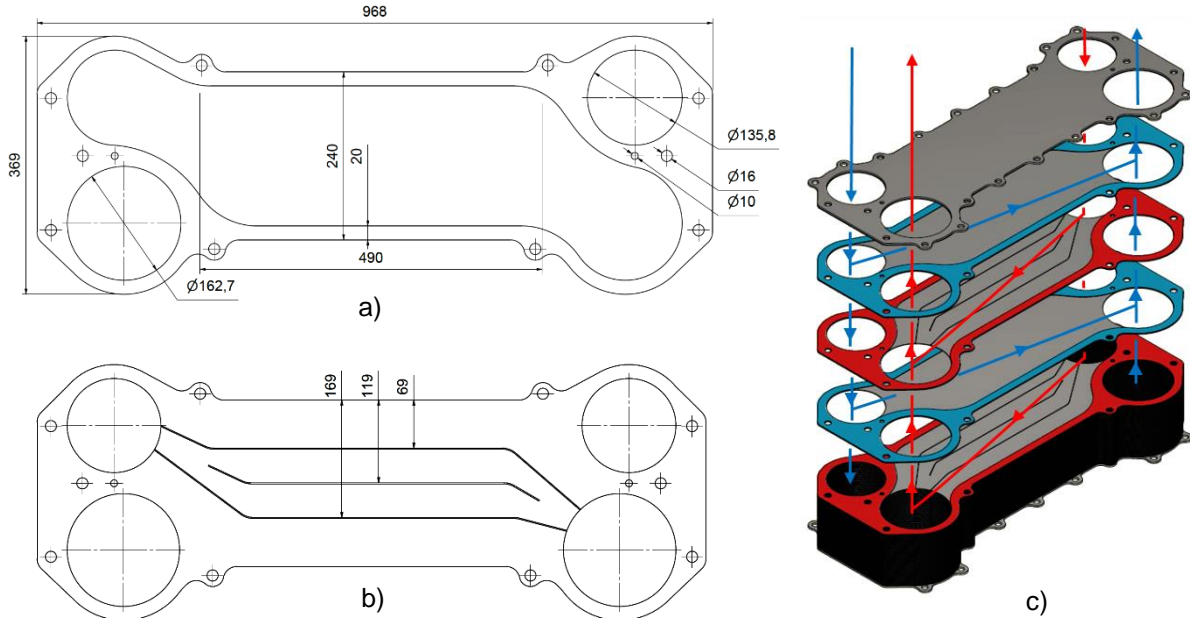


**Figure 4. a) Gasket Design, b) Hot Plate with Spacers, c) Exploded View of Recuperator**

The cost of 125 channel pairs was found to be too great for the available budget of the project. It was decided that an effectiveness of 0.92 could not be obtained, by reducing the number of channel pairs for the same channel length, without substantially increasing the pressure drop. It was decided to adapt the design, thereby sacrificing effectiveness for pressure drop and cost.

The number of channel pairs needed to be decreased however, this led to a pressure drop increase and to compensate for this, the channel height was increased. To arrive at a similar pressure drop to the original design, a constant pressure drop line was traced between the curves of differing channel heights (Figure 5(a)). With a channel height of 1.5 mm, the corresponding number of channel pairs was 25. This geometrical arrangement fell within the budget of the project. Consequently, the effectiveness was lowered to 0.6 (Figure 5(b)).

It can be observed, from this figure, how the effectiveness values increase rapidly for a lower amount of channel pairs and start to slow down at 50 - 75 channel pairs. Thereafter, to increase from an effectiveness value of approximately 0.85 to 0.9, with a channel height of 1.5, the number of channel pairs must increase by 50. This results in a 50% cost increase for a 5% effectiveness increase and marginal pressure decrease.

Decreasing the number of channel pairs resulted in the Reynolds number of the cold and hot-side flow being slightly above the critical laminar Reynolds number (around 2000 (White, 2009)). This resulted in a different Nusselt number and friction factor than the laminar case used before. The Nusselt number for this flow case, suggested by Shah & Sekulić (2003) is

$$Nu = (1.33 - Re/6000)Nu_{lam} + (-0.33 + Re/6000)Nu_{tur} \quad (7)$$

where the turbulent Nusselt number ( $Nu_{tur}$ ) is determined with the Dittus-Boelter relation. The friction factor suggested by White (2009) is

$$1/f^{1/2} = 2\log(0.64Re_{D_h}f^{1/2}) - 0.8 \quad (8)$$

where  $Re_{D_h}$  is the Reynolds number based on the hydraulic diameter of the channel and  $f$  is the friction factor. The pressure drops for the original design and the adapted design that was implemented, are presented in the Table 2. The overall pressure drop column includes the header pressure drops on both fluid sides. It can be noted that the increase in the pressure drops for the adapted geometry is marginal, even though the flow can be regarded as turbulent.

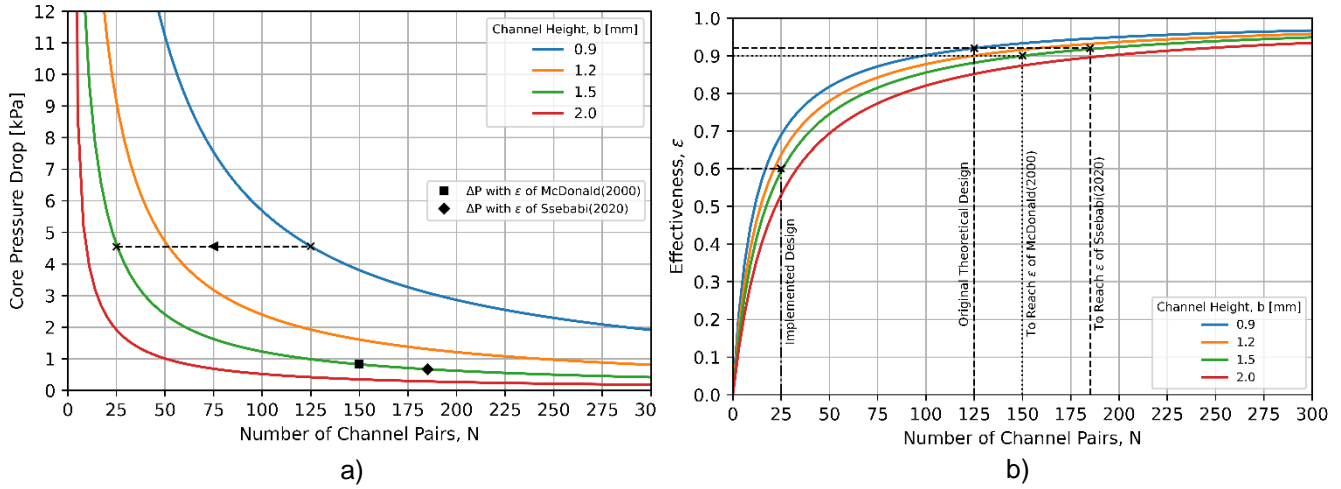


**Figure 5. a) Number of Channel Pairs vs Core Pressure Drop with Modified Geometry, b) Number of Channel Pairs vs Effectiveness with Modified Geometry**

**Table 2. Theoretical Pressure Drops of the Original and Implemented Design**

Geometries	$\Delta P_{cold,core}$ [kPa]	$\Delta P_{hot,core}$ [kPa]	Overall $\Delta P$ [kPa]
Original Design	1.64	3.32	4.96
Implemented Design	1.81	4.01	6.23

The gaskets, plates and spacers were laser-cut from the same material. The spacers were spot welded onto the plates with a low voltage to not burn through plate. There was no notable affect made on the quality of the reverse-side plate surface.

The sealant and application method utilised by Dellar (2019), was initially followed to seal the recuperator. Half the amount of water was used to thin the sealant. A pressure test was conducted on the sealed recuperator which revealed leaks in a multitude of places, including between the high and low pressure headers. It was decided to reseal the recuperator using a different sealant. Holts Firegum Exhaust Assembly Paste, which has a sufficiently long drying time and is heat-resistant up to 1000 °C, was selected. The newly sealed recuperator was cured at 100 °C over a weekend. A second pressure test was conducted, which revealed a significantly lower number of leaks that were difficult to detect. Compared to the relatively large flow rate that would be flowing through the recuperator during operation, the leak mass flow rate would be negligible. The clamped plate style design can be concluded to be leak inherent and it should be the designer's prerogative to decide on an acceptable limit. Finally, the method of attaching the recuperator to the MGT system is presented in Figure 6, below. The CAD (computer aided design) model of the system, developed by Ssebabi (2020), was adapted to include the recuperator.

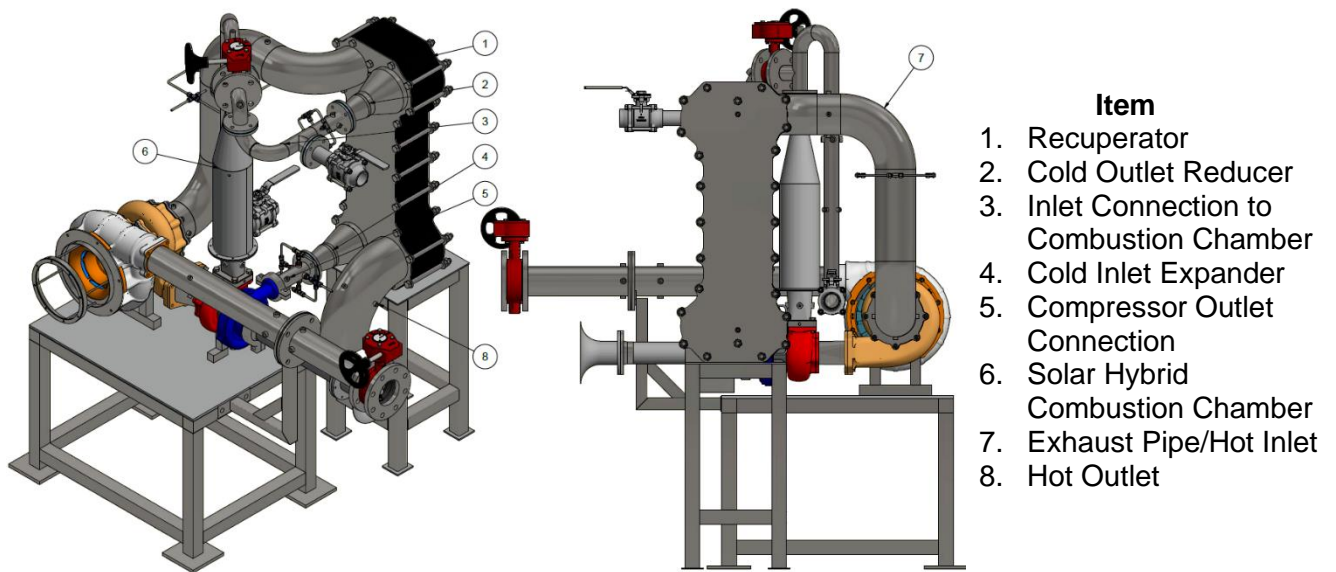


**Figure 6. Attachment Methodology**

#### 4. Experimental Results

The purpose of the experimental work was to connect the recuperator to the MGT system and to test its performance, characterised by effectiveness and pressure drop. How the system behaved in terms of turbocharger performance and operation was also a performance metric in the experimentation. From the findings of the heat loss analysis, it was decided not to insulate the recuperator. The testing periods were not long enough to justify the use of insulation. Tests were limited to three minutes each to ensure the longevity and safety of the MGT system.

The system was designed to be started in a decoupled mode of operation. This entails closing the valve to the inlet of the combustion chamber, while allowing the K31 compressor to vent to the atmosphere. A compressed air supply line feeds the combustion chamber and K31 turbine with flow during this process. Once the system has thermally soaked, a switch-over procedure is performed to get the system into a coupled mode of operation, where the compressor directly feeds the turbine with flow. This process can be found in the work of Ssebabi (2020).

It was found that during the switch-over procedure the compressed air line forced air back into the recuperator, increasing the back pressure and causing compressor surge. The K31 compressor could not supply a sufficient mass flow to sustain combustion once the compressed air start-up supply was shut-off. It was decided that the experimental testing would consist of obtaining recuperator temperatures and effectiveness values for different K31 shaft operating speeds, in a decoupled mode of operation. The results from only one of the target operating speeds will be discussed here. However, the general findings from the lower K31 shaft speed tests include:

- Due to the cold outlet temperature of the recuperator reaching or rising above 200 °C on start-up, it was decided to start thermally soaked tests with this temperature as the starting metric.
- To reach the same decoupled speed, a lower fuel mass flow rate was required for the tests starting at the 200 °C cold outlet condition. This was due the K31 turbine losing less heat to the walls of the machine, enabling more energy to be extracted from the flow, with a slightly lower fuel requirement.

- The effectiveness calculation was based off the hot side because this was the flow side that experienced the greatest temperature change, providing a limit to the heat transfer (Çengel & Ghajar, 2015).
- As the average temperature on the cold-side of the recuperator increased, the flow would increase in velocity due to a lower density. This would increase the pressure drop within the cold-side of the recuperator and impose a larger flow resistance, resulting in a greater back pressure on the compressor. An increase in compressor outlet pressure must result in a decreased mass flow rate to preserve the same shaft speed. This is due to the negative slope of the lower speed lines on the K31 compressor chart.
- A consequence of a decreased mass flow through the cold-side of the recuperator, was a decreased effectiveness. This was due to less heat being extracted from the hot-side per unit time, allowing the average hot-side temperature to increase.
- The average effectiveness increases as the K31 shaft speed increases and the maximum cold outlet temperature recorded increases by approximately 50 °C per 5,000 RPM increase.

Two tests were conducted where a K31 shaft speed of 55,000 was the target. In the second test the recuperator was pushed above the recommend maximum hot inlet temperatures stated in literature by using a slightly higher fuel mass flow rate. The temperature and effectiveness results for these tests are presented in Figure 7, while other test parameters are listed in Table 3. The aforementioned reduction in mass flow rate and increase in pressure during a test can be observed in Figure 8 and the corresponding gradual decrease in effectiveness can be seen in Figure 7(b).

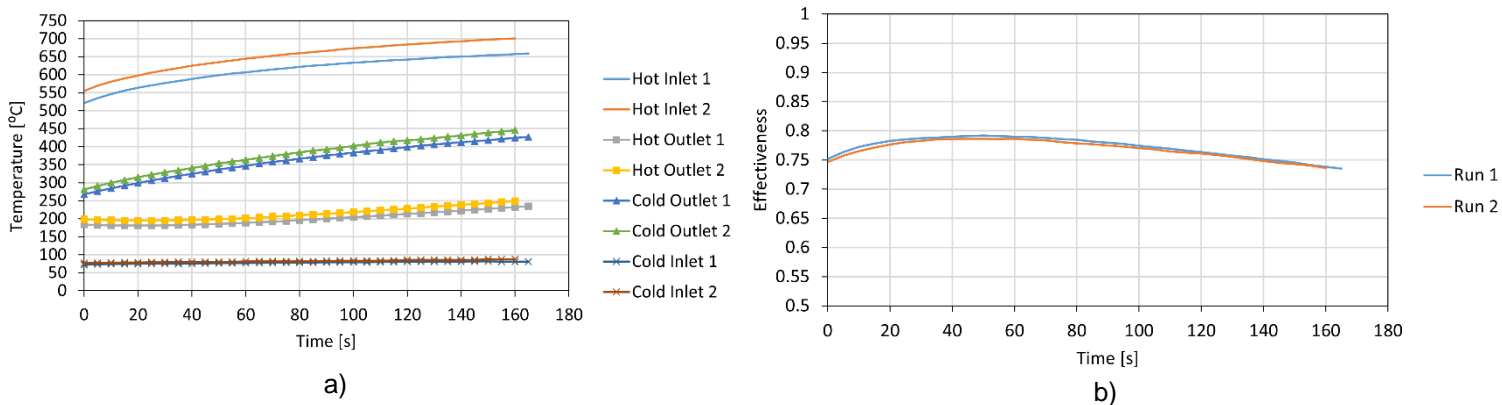


Figure 7. a) Temperature Results b) Effectiveness Results

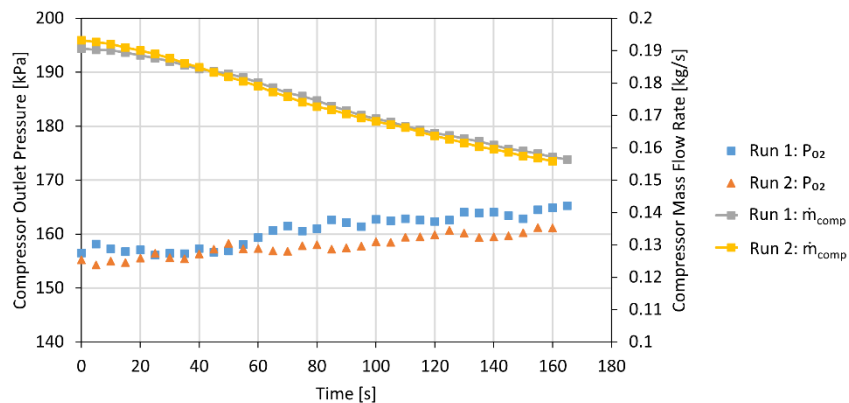
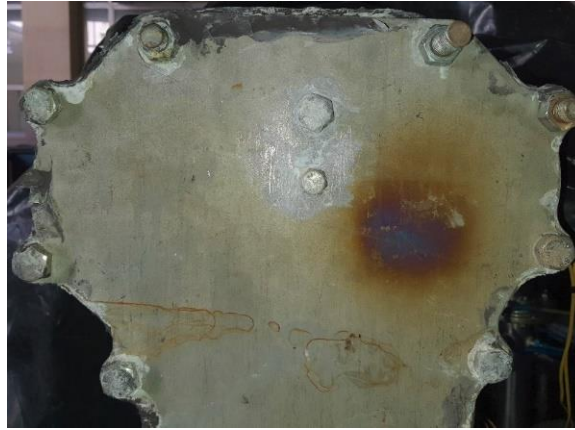


Figure 8. Compressor Outlet Pressure and Mass Flow Rate vs Time

**Table 3. Test Parameters**

Run	rp	TIT [°C]	$\dot{m}_a$ [kg/s]	$\dot{m}_{supp}$ [kg/s]	$\dot{m}_F$ [kg/s]	$N_{K31}$ [RPM]	$N_{K44}$ [RPM]
1	1.56	847	0.172	0.115	0.00502	56,204	13,432
2	1.59	793	0.172	0.114	0.00481	56,107	13,527

After the second test, thermal degradation, on the plate that closed the back of the recuperator, appeared on the hot-inlet header side (Figure 9). The thermal degradation was concentrated at a point or hot-pocket within the header, revealing that there was some form of flow maldistribution within the headers. Flow maldistribution within the headers would result in a larger pressure drop because the mass flow through the core of the recuperator is split unequally and most of the flow is forced through a smaller number of channels. With flow maldistribution present in the header, the maximum flow occurs in the last channel for a U-flow configuration (Shah & Sekulić, 2003). This explains the formation of the hot-pocket at the end of the hot inlet header. The degradation present on the outside of this plate may be indicative of the thermal degradation within the core of the recuperator. Therefore, it was confirmed that, for stainless steel recuperators, the hot inlet temperature must be kept below 650 °C.

**Figure 9. Thermal Degradation**

To verify the validity of the experimental results, a comparison was made between the theoretical effectiveness and the experimental effectiveness. The code that was used in development of the recuperator, was utilised to determine an analytical effectiveness under the experimental conditions. To represent the thermal properties of the exhaust gas adequately, carbon and hydrogen theta functions, proposed by Fielding & Topps (1959) were utilised in the theoretical model. The results are listed in Table 4 where it can be noted that there was a good correlation between the experimental and theoretical adiabatic results. The heat loss analysis results are included and revealed a higher hot-side effectiveness and lower cold-side effectiveness, as expected. However, the average value was close to both the experimental and adiabatic results.

**Table 4. Comparison of Recuperator Effectiveness Values**

Run	Experimental $\epsilon_{avg}$	Adiabatic $\epsilon$	HL $\epsilon_c$	HL $\epsilon_h$	HL $\epsilon_{avg}$
1	0.768	0.761	0.741	0.769	0.755
2	0.771	0.763	0.743	0.772	0.758

Due to the decoupled nature of testing, the pressure drops measured over the recuperator would be larger than normal operation and may be misleading. This is a result of the cold-side venting directly to atmosphere and the hot-side having a significantly larger pressure, compared to standard operation, downstream of the K44 turbine due to the compressed air supply pressure. To develop a pressure drop characteristic for this recuperator, a cold flow

pressure drop test was conducted. This provided a means of describing the pressure drop in terms of volume flow rate, which was useful because at a certain flow condition with a known mass flow rate, the density of the fluid could be used to calculate the volume flow rate. This can then be used to calculate the corresponding pressure drop. The approach provides a meaningful way of arriving at an expression that can be used in the modelling of the header maldistribution pressure drops in Flownex.

The K31 compressor was disconnected from the cold inlet to the recuperator and the compressed air supply line was directly attached to this inlet. This method of testing allowed the pressure drop over the cold side of the recuperator to be obtained directly, for a certain mass flow rate. It was deemed unnecessary to measure the cold flow pressure drop on the hot-side because both sides are geometrically identical, except for one flow channel less on the hot-side. Two tests were conducted to ensure the repeatability of the results. The theoretical calculation of the pressure drop over the core of the heat exchanger is of the same form as the one utilised in the plate heat exchanger element in Flownex. The theoretical pressure drop over the core of the heat exchanger, at the flow states measured in these tests, was subtracted from the overall experimental pressure drop. This would directly result in the component of the header pressure drop and other losses in the recuperator, which Flownex does not calculate. The relation for the header pressure drops is given by:

$$\Delta P = 7144.8\dot{V}^3 - 1874.3\dot{V}^2 + 246.73\dot{V} + 0.1679 \quad (9)$$

## 5. Flownex Modelling

The MGT system developed by Ssebabi (2020) was modelled in Flownex and was verified analytically, based on the same experimental data. Additionally, the decoupled operation of the recuperated MGT system was modelled and a partially bypassed recuperator setup was proposed to allow the system to self-sustain.

In order to model the recuperated MGT system, a standard MGT model had to be developed first (Figure 10). The experimental data from Table 1 was used as an operating point to model in Flownex. The Flownex layout for the system is presented in Figure 10 below. The pressure drop over the combustion chamber was modelled with the User Defined Pressure Drop component. The pressure loss characteristic for the newly installed SHMGT combustion chamber was obtained during the experiments that were used to establish a realistic operating point for the recuperator. This characteristic curve was used within the Flownex component. The TIT (turbine inlet temperature) was adjusted to the experimental value with the use of an Iterative Script component and a Flow Resistance component. Saravanamuttoo, et al., (2017) suggest that the combustion efficiency can be adequately represented in terms of the ratio of actual temperature rise to theoretical temperature rise, over the combustion chamber. The combustion efficiency can then be represented by

$$\eta_{comb} = \frac{\Delta T_{actual}}{\Delta T_{theoretical}} = \frac{T_{TIT,actual} - T_{CCIT,actual}}{T_{TIT,theoretical} - T_{CCIT,actual}} \quad (10)$$

where CCIT is the combustion chamber inlet temperature. Due to the large area to volume ratio of the K44 turbine, the gas temperature leaving the K44 turbine was lower than that predicted analytically and with Flownex. Fenner (2022) found that the K44 machine needed an extended period of experimentation to heat soak. As a result, a portion of the thermal energy of the gas was being lost to the casing. To account for some of this energy lost, Composite Heat Transfer elements were incorporated into the model before each of the turbines. The physical characteristics of the turbines and ambient conditions were input to this component. The results from this Flownex model are presented in Table 5.

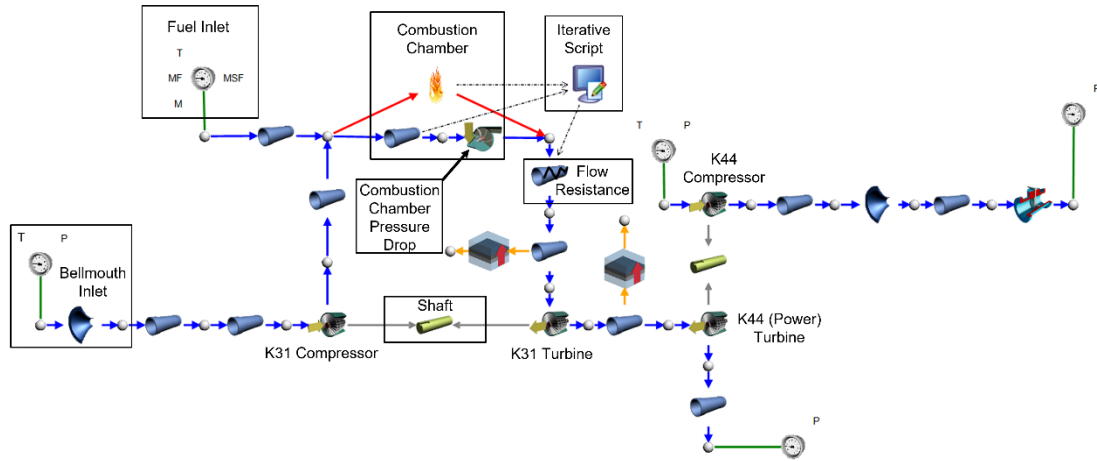


Figure 10. Standard MGT Flownex Network

Table 5. Performance Parameters of Standard MGT Model

$N_{K31}$ [RPM]	$N_{K44}$ [RPM]	$W_{pt}$ [kW]	$\eta_{th}$ [%]	$\eta_{comb}$ [%]	Exhaust Temperature [°C]	HL K31 [kW]	HL K44 [kW]
61,915	20,814	4.16	2.9	84	698	1.65	2.04

The heat loss from the turbine casings of the turbochargers is on a comparable level to the power output from the power turbine. Without the heat loss in the turbochargers, the exhaust temperature would be approximately 10 °C higher, however the experimental exhaust temperature remains largely lower.

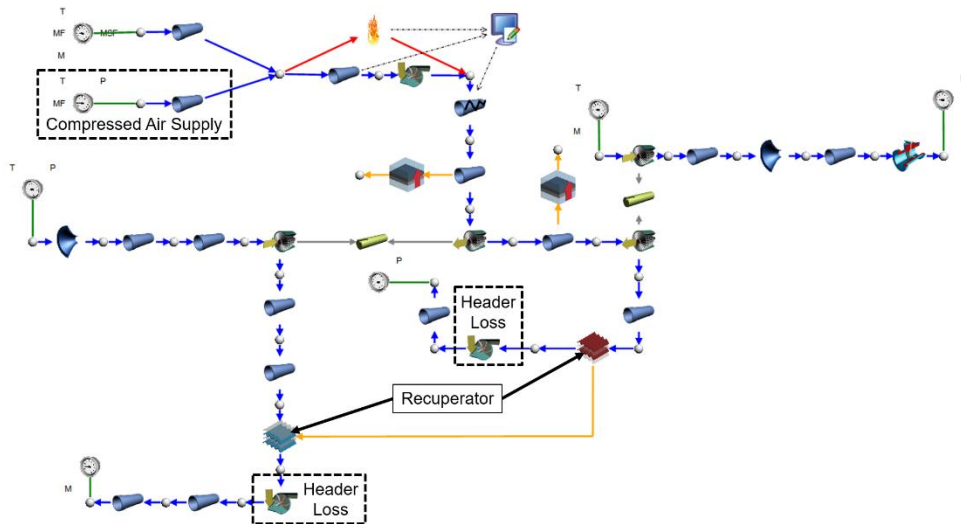
A Flownex model of the decoupled recuperator MGT setup was developed to confirm the experimental and analytical effectiveness results. Additionally, the pressure drop over the core of the recuperator could then be confirmed to lie within the expected analytical operating range, indicating that the remainder of the pressure drop can be accounted for in the headers. The header pressure drops were incorporated with the use of the User Defined Pressure Drop component. The operating point used in the Flownex model was based on the first run in Table 3. The Flownex network for the decoupled operation of the system is presented in Figure 11.

Table 6. Decoupled Flownex Results

$W_{pt}$ [kW]	$\epsilon$ [-]	$\eta_{comb}$ [%]	Exhaust Temperature [°C]	Cold Outlet Temperature [°C]	$\Delta P_{core,cold}$ [kPa]	$\Delta P_{core,hot}$ [kPa]
3.1	0.77	92.6	740	589	1.94	4.03

The work output was lower than the coupled operating case due to a lower mass flow rate from the compressed air supply system and a lower TIT. To reach the experimental TIT, a combustion efficiency of 92.6% was needed in the iterative script. This efficiency can be observed to be higher than the coupled operating case, which suggests that the mixing conditions of the fuel and air might have been enhanced by the compressed air supply line during testing. Additionally, with a lower mass flow rate, the air-fuel mixture was less lean, resulting in the experimental flame temperature approaching the adiabatic temperature.

Like the standard MGT model, the experimental K44 exhaust temperature in decoupled operation was higher than the simulated result. Consequently, the simulated cold-side outlet temperature of the recuperator was higher than the experimental result. However, the resulting effectiveness value was in close agreement with the analytical and experimental results. Additionally, the pressure drop over the core of the recuperator can be observed to be within the realm of the analytical values in Table 2. Therefore, the decoupled simulation confirms the validity of the experimental and analytical results in terms of pressure drop and effectiveness.



**Figure 11. Decoupled Flownex Network**

An additional Flownex model was developed where a pipe element was placed in parallel to the cold side of the recuperator. A valve component was added to this pipe to regulate the mass flow through the cold side of the recuperator. Similarly, a pipe and valve were fitted upstream of the hot-side of the recuperator that enabled some bypass flow to the atmosphere. A parametric study was conducted on both valve opening angles to determine the best combination. Parameters such as recuperator pressure drop, compressor and turbine efficiency, combustion chamber pressure drop and the power turbine's work output, were analysed in this process. It was found that a cold-side valve opening angle of  $55^\circ$  and a hot-side opening angle of  $30^\circ$  were the best combination.

During the parametric study, it was found that increased CCITs incurred a large combustion chamber pressure drop. An increase in temperature upstream of the combustion chamber would decrease the density of the flow and increase the volume flow rate, thereby increasing the pressure drop over the combustion chamber. With the operating state listed in Table 1, an increase of the CCIT up to  $400^\circ\text{C}$ , which was the recuperator's cold outlet temperature reached during decoupled testing, the pressure drop over the combustion chamber would be approximately 55 kPa. Therefore, the current SHMGT combustion chamber is not sized correctly to accommodate high temperature flows without incurring an unacceptable pressure drop. This may be another explanation as to why the MGT system could not self-sustain; the combination of the cold and hot-side recuperator pressure drops and a substantially increased combustion chamber pressure drop were too excessive for the K31 turbine to overcome.

The work output of the power turbine was found to be half of the standard MGT operation's work output, consequently dropping the thermal efficiency by a percentage point. However, the fuel mass flow rate was halved. After the flow from the cold-side of the recuperator mixed with the partially bypassed flow from the compressor, the temperature of the combined flow entering the combustion chamber was  $170^\circ\text{C}$ . This was not much of an

improvement from the 99 °C CCIT during standard operation. Therefore, the recuperator is parasitic to the operation of the MGT system in this state. An improved design of the recuperator itself is needed.

## 6. Improved Recuperator Design

To prevent leakage and improve the assembly process of the recuperator, a different method of sealing must be adopted. Instead of using a stainless-steel gasket with a high temperature sealant, a BAR302 gasket can be used. This gasket material can withstand a maximum temperature of 650 °C (Gasket & Shim Industries, 2019), which coincides conveniently with the maximum recommended allowable inlet temperature to the recuperator. A comparison of the cost between the BAR302 gasket and a stainless steel gasket, with sealant, revealed that the BAR302 gasket was the more expensive option. However, it can be argued that the expense is outweighed by the benefits. The assembly of the recuperator will become truly modular, where the recuperator can be unclamped and re-clamped without breaking the seal. When assembling the recuperator, a pressure test can be conducted at certain assembly intervals to isolate a leak, if there is one. Additionally, the gaskets can be individually replaced without having to reseal the entire recuperator.

To prevent flow maldistribution in the recuperator, an improved header design must be implemented. The improvement of the flow distribution within the header can be obtained through the variation of the header diameter throughout its length. This can be achieved in two ways. The first is where a deflector plate is cut and bent into the shape of a partial circular cone, based on the header geometry. The plate will need to make some angle,  $\theta$ , with the vertical wall of the header. This is a quick and inexpensive method, where a few plates can be cut with differing setting angles and be tested to determine which angle will give the lowest pressure drop. Experimentation would involve unclamping the top plate of the recuperator, inserting the plate into the header and re-clamping the recuperator. The more difficult, second way is to redesign the header based on a function that describes the optimal curve for guiding the flow through the header and maintaining flow uniformity. This would require a specific assembly order of plates and gaskets. During the design the size of the inlet diameter would need to be decreased in a piece-wise manner, which may present itself as a tedious process. A schematic of both header designs is presented in Figure 12. This header design improvement was inspired by the work done by Zhang, et al. (2022).

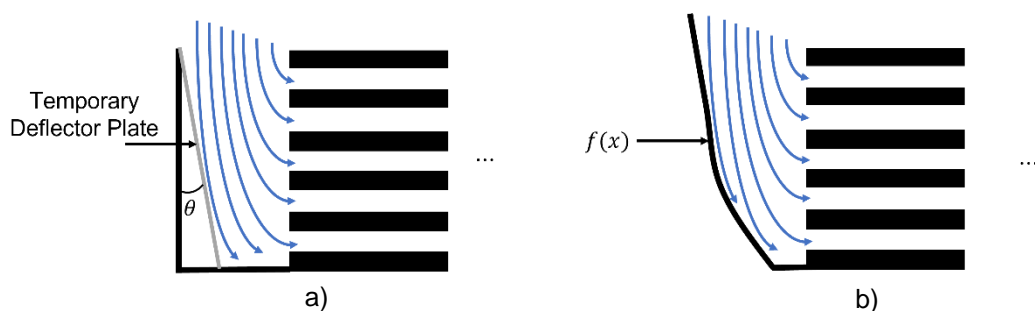


Figure 12. a) Linear Deflector Plate b) Header Design Governed by a Function

## 7. Conclusions and Recommendations

Although the MGT system could not self-sustain, valuable insight was found in the operation of the turbochargers in reaction to the incorporation of the recuperator. The effectiveness and pressure drop of the recuperator could still be obtained under a decoupled mode of operation. Good correlation between analytical, experimental and the simulated results was

found. Additionally, it was found that a revised combustion chamber design was needed to accommodate for a higher temperature inlet flow. It was confirmed that the maximum temperature limit for the operation of a stainless-steel recuperator, is 650 °C. Thermal degradation starts appearing above this limit. This temperature limit coincides with that of the proposed BAR302 gasket. The inlet header must be optimised to eliminate flow maldistribution. A CFD (computational fluid dynamics) simulation can be conducted with different designs to determine the best geometry for this application. It is recommended that entirely different recuperator designs be investigated to determine which are the most feasible with regards to cost, assembly and implementation method, pressure drop and effectiveness.

## References

- Dellar, K. E., 2019. *Clamped-plate Style Recuperator for a Small-scale Solar Thermal Brayton Cycle using High-temperature Sealant*, University of Pretoria: Department of Mechanical and Aeronautical Engineering Faculty of Engineering, Built Environment and Information Technology.
- Fenner, C. C., 2022. *Improved modeling of a Micro Gas Turbine for Solar-Hybrid Application*, Stellenbosch University: Department of Mechanical and Mechatronic Engineering.
- Fielding, D. & Topps, J. E. C., 1959. Thermodynamic Data for the Calculation of Gas Turbine Performance. *Aeronautical Research Council Reports and Memoranda*, 3099(13), pp. 211-228.
- Gasket & Shim Industries, 2019. *BAR302 - Exhaust Gasket Material*. Cape Town: Gasket & Shim.
- Kays, W. M. & London, A. W., 2018. *Compact Heat Exchangers*. 3rd ed. United States of America: Scientific International.
- le Roux, W., Bello-Ochende, T. & Meyer, J., 2011. *Maximum Net Power Output of the Recuperative Open and Direct Solar Thermal Brayton Cycle*. Washington D.C., ASME.
- le Roux, W. & Meyer, J., 2015. *Modeling the Small-scale Dish-mounted Solar Thermal Brayton Cycle*. Cape Town, AIP.
- McDonald, C. F., 2000. Low-cost compact primary surface recuperator concept for microturbines. *Applied Thermal Engineering*, 20(5), pp. 471-497.
- Nellis, G. F. & Pfotenhauer, J. M., 2005. Effectiveness-NTU Relationship for a Counterflow Heat Exchanger Subjected to an External Heat Transfer. *Journal of Heat Transfer*, 127(9), pp. 1071-1073.
- Oppong, F., 2016. *Micro Gas Turbine Performance Evaluation*, Stellenbosch : Department of Mechanical and Mechatronic Engineering, Stellenbosch University.
- Saravanamuttoo, H. I. H. et al., 2017. *Gas Turbine Theory*. 7th ed. United Kingdom: Pearson.
- Shah, R. & Sekulić, D., 2003. *Fundamentals of Heat Exchanger Design*. 1st ed. United States of America: John Wiley & Sons.
- Ssebabi, B., 2020. *Development of a Micro Gas Turbine for Central Receiver Concentrating Solar Power Systems*, Stellenbosch University: Department of Mechanical and Mechatronic Engineering.
- White, F. M., 2009. *Fluid Mechanics*. 4th ed. United States of America: WCB/McGraw-Hill.
- Young, W. C. & Budynas, R. G., 2002. *Roark's Formulas for Stress and Strain*. 7th ed. United States of America: McGraw-Hill.
- Zhang, K. et al., 2022. The Optimization of the Structure of PCHE Inlet Header Based on Flow Distribution Uniformity. *Applied Sciences*, 12(13).
- Çengel, Y. A. & Ghajar, A. J., 2015. *Heat and Mass Transfer: Fundamentals and Applications*. 5th ed. United States of America: McGraw-Hill Education.